

6 Soil heterogeneity

J.C. van Dam, R.F.A. Hendriks

6.1 Introduction

In many cases SWAP is used at field scale level, which can be viewed as a natural basic unit of larger regions. Most natural or cultivated fields have one cropping pattern, soil profile, drainage condition and management scheme. This information comes increasingly available in geographical data bases. Geographical information systems can be used to generate input data for field scale models, to run these models for fields with unique boundary conditions and physical properties, and to compile regional results of viable management scenarios. The regional scale is of most interest to water managers and politicians. In order the use SWAP at field scale level, we should consider the natural soil heterogeneity within a field. SWAP has options to accommodate hysteresis in the retention function, spatial variability of soil hydraulic functions, preferential flow in water repellent soils and in soils with macropores.

6.2 Hysteresis

Hysteresis refers to non-uniqueness of the $\theta(h)$ relation and is caused by variations of the pore diameter (inkbottle effect), differences in radii of advancing and receding meniscus, entrapped air, thermal gradients and swelling/shrinking processes (Hillel, 1980; Feddes et al., 1988). Gradual desorption of an initially saturated soil sample gives the main drying curve, while slow absorption of an initially dry sample results in the main wetting curve. In the field partly wetting and drying occurs in numerous cycles, resulting in so-called drying and wetting scanning curves lying between the main drying and the main wetting curves (Figure 27).

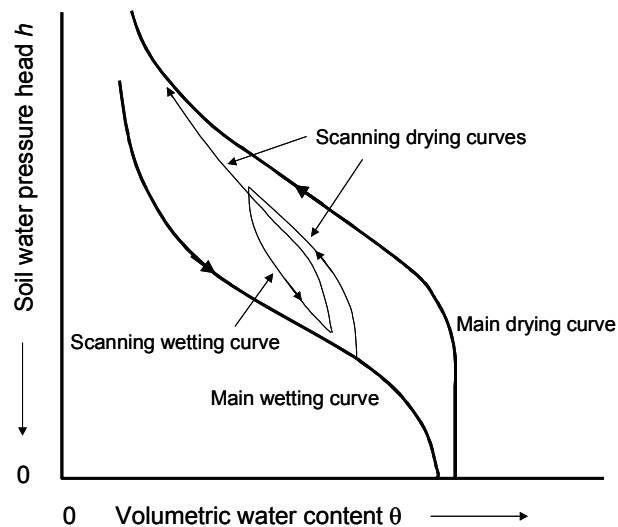


Figure 27 Water retention function with hysteresis, showing the main wetting, main drying and scanning curves

In simulation practice, often only the main drying curve is used to describe the $\theta(h)$ relation. This is mainly due to the time and costs involved in measurement of the complete $\theta(h)$ relationship, including the main wetting, the main drying and the scanning curves, especially in the dry range. For instance, a generally applied soil hydraulic data base in The Netherlands, known as the Staring series (Wösten et al., 1994), contains only $\theta(h)$ data of the main drying curve. Nevertheless, it is obvious that the simulation of infiltration events with the main drying curve can be inaccurate. Kaluarachchi and Parker (1987) showed that during infiltration the type of boundary condition at the soil surface determines the effect of hysteresis. A head-type boundary condition at the soil surface has more influence than a flux-type boundary condition. Dirksen (1987) could not explain his detailed experimental data on root water uptake in saline conditions without taking into account hysteresis. Hopmans et al. (1991) showed in case of trickle and furrow irrigation that hysteresis affects the water balance, although these effects were overwhelmed by spatial variability of the soil hydraulic functions.

To circumvent the tedious laboratory analysis, empirical hysteresis models with a limited number of parameters have been developed. Jaynes (1984) compared four of these models, which use the main wetting and main drying curve to generate scanning curves. None of the models was consistently better than the others for simulating primary wetting or drying curves for three test soils. Also each model performed equally well when used as part of a numerical model for simulating hysteretic flow. Scott et al. (1983) derived scanning curves by rescaling the main wetting or the main drying curve to the actual water content. Among others, Kool and Parker (1987) obtained acceptable results with Scott's method in the case of eight soils. The scaling method of Scott has been implemented into SWAP.

The main drying and main wetting curve should be measured in the laboratory and are described analytically with the Mualem-van Genuchten parameters (α , n , θ_{res} , θ_{sat} , K_{sat} , and λ) according to Eqs. (2.20) and (2.22). Some of the parameters describing the main wetting and main drying curve are related. We will assume θ_{res} and θ_{sat} to be equal for both curves. In general θ_{sat} will be somewhat less than porosity due to air entrapment under field conditions with intensive rainfall. Usually the $K(\theta)$ function shows only minor hysteresis effects. As Eq. (2.22) shows, this can be achieved by choosing for the main wetting and main drying curve a common value for n . Ultimately the two curves only differ in the parameter α , as depicted in Figure 28.

The scanning curves are derived by linear scaling of either the main wetting or main drying curve, such that the scanning curve includes the current θ - h combination and approaches the main wetting curve in case of a wetting scanning curve and the main drying curve in case of a drying scanning curve.

Figure 28A shows the scaling principle in case of a drying scanning curve. Based on its wetting and drying history, at a certain time and depth the soil shows an actual water content θ_{act} at the soil water pressure head h_{act} . The valid drying scanning curve should pass through the point (θ_{act}, h_{act}) , and approach the main drying curve at smaller water contents. We may define θ_{md} as the water content of the main drying curve at h_{act} , and θ_{sat}^* as the saturated water content of the drying scanning curve. Linear scaling of the main drying curve with respect to the vertical axis $\theta = \theta_{res}$ gives (Figure 28A):

$$\frac{\theta_{sat}^* - \theta_{res}}{\theta_{sat} - \theta_{res}} = \frac{\theta_{act} - \theta_{res}}{\theta_{md} - \theta_{res}} \Rightarrow \theta_{sat}^* = \theta_{res} + (\theta_{sat} - \theta_{res}) \frac{\theta_{act} - \theta_{res}}{\theta_{md} - \theta_{res}} \quad (6.1)$$

The only unknown in Eq.(6.1) is θ_{sat}^* , which can be directly solved. The drying scanning curve is accordingly described with the parameters $(\alpha_{dry}, n, \theta_{res}, \theta_{sat}^*)$. As long as the soil keeps drying, this drying scanning curve is valid.

The opposite occurs when the soil gets wetter. Again we start from the arbitrary actual water content θ_{act} at the soil water pressure head h_{act} , and now define θ_{mw} as the water content of the main wetting curve at h_{act} , and θ_{res}^* as the residual water content of the wetting scanning curve.

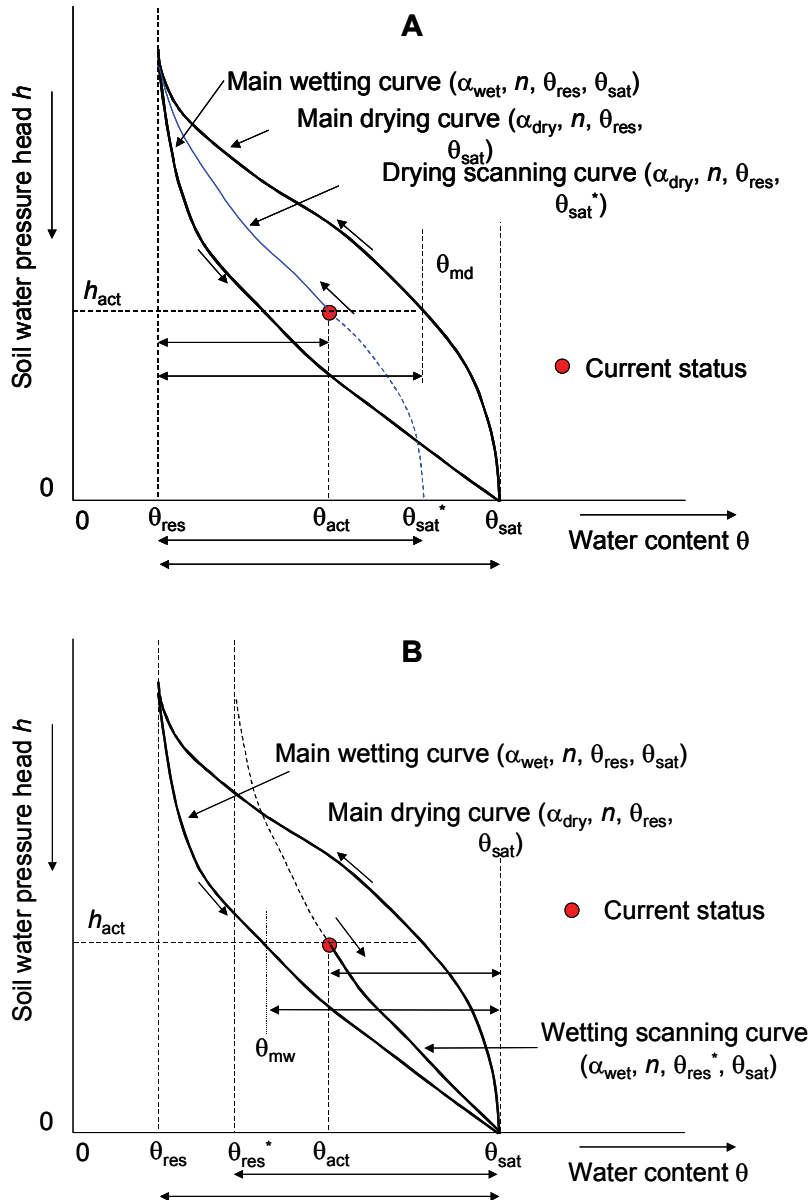


Figure 28 (A) Linear scaling of the main drying water retention curve in order to derive a drying scanning curve; (B) Linear scaling of the main wetting water retention curve in order to derive a drying wetting curve.

Linear scaling of the main wetting curve with respect to the vertical axis $\theta = \theta_{\text{sat}}$ gives (Figure 28B):

$$\frac{\theta_{\text{sat}} - \theta_{\text{res}}^*}{\theta_{\text{sat}} - \theta_{\text{res}}} = \frac{\theta_{\text{sat}} - \theta_{\text{act}}}{\theta_{\text{sat}} - \theta_{\text{mw}}} \Rightarrow \theta_{\text{res}}^* = \theta_{\text{sat}} - (\theta_{\text{sat}} - \theta_{\text{res}}) \frac{\theta_{\text{sat}} - \theta_{\text{act}}}{\theta_{\text{sat}} - \theta_{\text{mw}}} \quad (6.2)$$

From Eq.(6.2), θ_{res}^* can be directly solved. The wetting scanning curve is accordingly described with the parameters $(\alpha_{\text{wet}}, n, \theta_{\text{res}}^*, \theta_{\text{sat}})$, and is valid as long as the soil keeps wetting. As the wetting-drying history is different at each soil depth, each node may show a different scanning curve. The unique $K(\theta)$ relation of a soil layer always follows from the parameter set $(n, \theta_{\text{res}}, \theta_{\text{sat}}, K_{\text{sat}}, \lambda)$ according to Eq. (2.22).

<i>Model input</i>			
<i>Variable</i>	<i>Code</i>	<i>Description</i>	<i>Default</i>
α_{dry}	ALFA	shape parameter alfa of main drying curve (cm^{-1})	
α_{wet}	ALFAW	shape parameter alfa of main drying curve (cm^{-1})	$\alpha_{\text{wet}} = 2 \alpha_{\text{dry}}$
	SWHYST	initial condition wetting or drying	drying
	TAU	minimum pressure head difference to change wetting-drying (cm)	0.2

6.3 Scaling of soil hydraulic properties

6.3.1 Introduction

Most models of the unsaturated zone are one-dimensional. The hydrological and drainage problems that have to be modelled however, are two- or three-dimensional and thus have a spatial component, be it a local or a regional one. If the area is homogeneous in all its components, a point simulation is representative of an entire region. The soil however, is never homogeneous, but is subject to spatial variability. It is not feasible to model the actual heterogeneity in a deterministic way as this would require enormous amounts of data and too much computational effort (Hopmans and Stricker, 1989). As the flow and transport processes in the unsaturated zone are strongly non-linear, in general the mean input of soil hydraulic functions will deviate from the areal mean water and solute balance. Various theoretical frameworks have emerged to model water flow and solute transport in heterogeneous soils. The most important concepts are summarized below.

One option to deal with the variability of the soil hydraulic and transport parameters is to treat them as random variables. Spatial patterns of these parameters can be produced by drawing from the statistical distributions of the parameters. This method (distributed modeling) is computationally very demanding, since numerous fields have to be simulated to produce the mean and standard deviation of the variables of interest. A simpler approach is to assume vertical flow only (which is quite realistic for unsaturated flow) and view the field as a collection of non-interacting columns with variable properties but without horizontal variations (Bresler and Dagan, 1981). This greatly reduces calculation time.

The geometrically similar media scaling technique (Miller and Miller, 1956) is an efficient way to describe the variability of the soil hydraulic properties. In its simplest form, the

technique assumes that the $\theta(h)$ and $K(\theta)$ functions at any point in the field are linear transformations of those at any other point. This technique will be described in the next Par..

Another much used approach is to view the soil as a combination of two or more parallel, homogeneous flow domains with contrasting soil properties (multi-domain models). Flow is vertical in each domain. The solute behavior is the result of the size of each domain and the function that defines solute exchange between domains (usually a simple diffusion process). Even with simple exchange functions, this type of models can produce a wide variety of breakthrough curves (Van Genuchten and Wierenga, 1976; Gerke and Van Genuchten, 1993). In SWAP the mobile-immobile concept is employed to mimic this type of flow and transport in water repellent soil (Par. 6.4). The fast and slow soil water flow in case of cracked clay soils is approached in SWAP employing the shrinkage characteristic and macropore flow theory (Par. 6.5).

6.3.2 Similar media scaling

Miller and Miller (1956) used the concept of geometrically similar media to deduce macroscopic equations governing the viscous flow phenomena. They showed that the variability in both the $\theta(h)$ and $K(\theta)$ relation might be described by just one dimensionless scale factor. The scale factor ρ_i at a certain location i is equal to:

$$\rho_i = \frac{\lambda_i}{\lambda_{\text{ref}}} \quad (6.3)$$

where (see Figure 29) λ_i is a characteristic length at location i , and λ_{ref} is the same characteristic length of a reference soil. Then, applying theory of capillary retention, if the soil at location i and the reference soil have the same water contents, their pressure heads are related according to:

$$h_i = \frac{h_{\text{ref}}}{\rho_i} \quad (6.4)$$

Using Poiseuille's law and again at the same water content in both soils, the hydraulic conductivities are related as:

$$K_i = \rho_i^2 K_{\text{ref}} \quad (6.5)$$

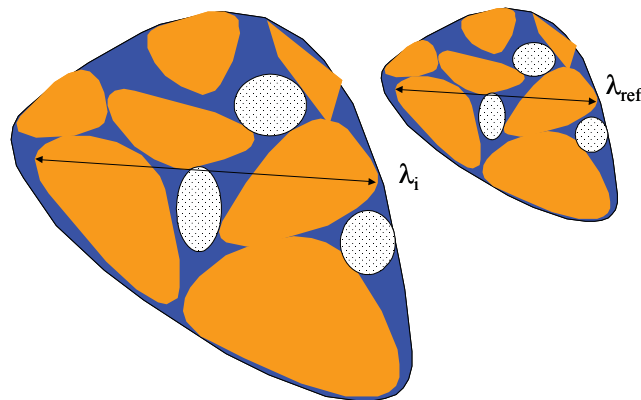


Figure 29 Characteristic lengths λ_i in geometrically similar media (Miller and Miller, 1956)

Natural soils will to some degree deviate from geometrically similar media. This is clear when we consider the saturated water content. If the similar media concept would apply strictly, the saturated water content should be the same for all soils. We know this is not the case. Jury et al. (1987) point out that due to dissimilarity, scaling of different soil properties, e.g. h and K , might result in different statistical properties of each scale factor's distribution. Youngs and Price (1981) measured microscopic characteristic lengths for porous materials ranging from glass beads and washed sands to sieved arable soils. They concluded that even for dissimilar soils the scaling concept is a good approximation.

In order to derive scale factors ρ_i and their statistical distribution, one should have $\theta(h)$ and $K(\theta)$ data of a series of soil samples. Clausnitzer et al. (1992) developed an efficient program for scaling $\theta(h)$ and $K(\theta)$ data of a series of soil samples. In their scaling approach, first a mean curve is fit to all the data available. Because natural soils don't have identical porosities, h and k are written as functions of the relative saturation $\theta/\theta_{\text{sat}}$ rather than as functions of the volumetric water content θ . In the second step, the corresponding set of scale factors is calculated for each soil sample. The scaled hydraulic data ($h_i\rho_i$ and K_i/ρ_i^2 , respectively) coalesce and allow an improved calculation of the mean curve. Therefore in the next step a new mean curve is fitted through the scaled hydraulic data, after which the scale factors are determined again. These steps are repeated until both the mean curve and the scale factors converge. Finally the stochastic distribution of the scale factors (generally log-normal), its mean and standard deviation are calculated.

Scaling is generally applied to determine the variability of the water balance components due to spatial variation of $\theta(h)$ and $K(\theta)$ (e.g. Peck et al., 1977; Hopmans and Stricker, 1989). SWAP will generate the water and solute balance for each scale factor that is provided. In areas without surface runoff, scaling might also be used to derive an equivalent curve for a field or a catchment (Feddes et al., 1993, Kim, 1995).

<i>Model input</i>			
<i>Variable</i>	<i>Code</i>	<i>Description</i>	<i>Default</i>
	NSCALE	number of scale factors and SWAP simulations (-)	
ρ_i	SOILI	NSCALE scale factors for each soil layer (-)	

6.4 Mobile/immobile flow

6.4.1 Introduction

In field soils soil water may bypass large parts of the unsaturated soil domain. This phenomenon is generally called preferential flow and has a large effect on the leaching of nutrients, salts and pesticides to the saturated zone. Preferential flow can be caused by macropores in structured soils (Par. 6.5) or by unstable wetting fronts in unstructured soils that originate from soil layering, air entrapment and water repellency (Raats, 1973; Ritsema et al., 1993). In SWAP attention is paid to water repellency, which is attributed to organic coatings of soil particles, to organic matter and to specific micro flora. Water repellency is widespread in dry top soils and can be quantified by water drop penetration time tests (Krammes and DeBano, 1965; Dekker and Jungerius, 1990). More than 75 % of the

cropland and grassland top soils in the Netherlands are slightly to extremely water repellent, whereas more than 95 % of the top soils in nature reserves are strongly to extremely water repellent (Dekker and Ritsema, 1994).

De Rooij (1996) provides an overview of theories and experiments with respect to preferential flow due to water repellency. The same author performed an extensive lysimeter experiment which showed the large heterogeneity of water and solute fluxes at the 5 cm scale. De Rooij (1996) developed an analytical three region model, which could be applied to the collected lysimeter data, but which is less suitable for fields with transient flow and fluctuating groundwater levels. A large amount of field data and water repellency phenomena have been collected by Dekker (1998) and Ritsema (1998).

Numerically, flow in water repellent soil might be simulated with a dual-porosity model as has been used for macropores in structured soils (Gerke and Van Genuchten, 1993; Saxena et al., 1994). However, the water exchange between the mobile and immobile domains in the case of water repellent soils is difficult to simulate. Also field observations show a time dependent preferential flow path volume (Ritsema and Dekker, 1994) while dual-porosity models assume a constant volume of the preferential flow path. Another limitation of dual-porosity models is that they require twice as many soil physical parameters as single porosity models.

Another approach is the *mobile-immobile concept*. This concept has been used to explain accelerated breakthrough in the case of steady state solute transport (De Smedt and Wierenga, 1979; Van Genuchten and Wagenet, 1989). Van Dam et al. (1990, 1996) extended the mobile-immobile concept to both water flow and solute transport and to transient flow conditions. Their concept of preferential flow is easy to conceive, uses a limited number of physically based and easy to measure parameters (e.g. the soil volume fraction in which water is mobile), is applicable to transient flow conditions and can relatively easily be implemented in current one-dimensional soil water flow and solute transport codes. The concept has been applied to bromide tracer experiments in water repellent soils in lysimeters (Saxena et al., 1994) and in field soils (Van Dam et al. 1990, 1996). In the next Par.s we elaborate on the mobile-immobile concept for soil water fluxes and solute transport as implemented in SWAP.

6.4.2 Water flow

Usually in the laboratory, when measuring the retention function and the hydraulic conductivity curve, soil samples are first brought to saturation and during the experiment relatively long equilibrium times are allowed. These conditions suppress effects of water repellency. The soil hydraulic functions measured in the laboratory will be denoted as $\theta_{lab}(h)$ and $K_{lab}(h)$.

In the field, immobile soil domains may occur either as large, separate volumes (Figure 30) or as numerous small volumes corresponding to less accessible pores. We will assume that the soil hydraulic functions as measured in the laboratory are valid in the preferential flow domains. A second assumption is that the water content in the immobile region, θ_{im} ($\text{cm}^3 \text{cm}^{-3}$) remains constant in time. Then the bulk field water retention function $\theta_{bulk}(h)$ can be calculated as (Figure 30):

$$\theta_{\text{bulk}}(h) = F_{\text{mob}}\theta_{\text{lab}} + (1 - F_{\text{mob}})\theta_{\text{im}} \quad (6.6)$$

where F_{mob} equals the mobile fraction of the soil volume ($\text{cm}^3 \text{cm}^{-3}$) through which flow actually occurs. The factor F_{mob} can roughly be estimated by visual observation of dry and wet spots in the field shortly after precipitation, and more accurately with tracer colour tests, e.g. with iodide (Van Ommen et al., 1989b) or Brilliant Blue (Flury and Flühler, 1995), with a disc permeameter in combination with a tracer (Clothier et al., 1992), or by model calibration (Van Dam et al., 1990).

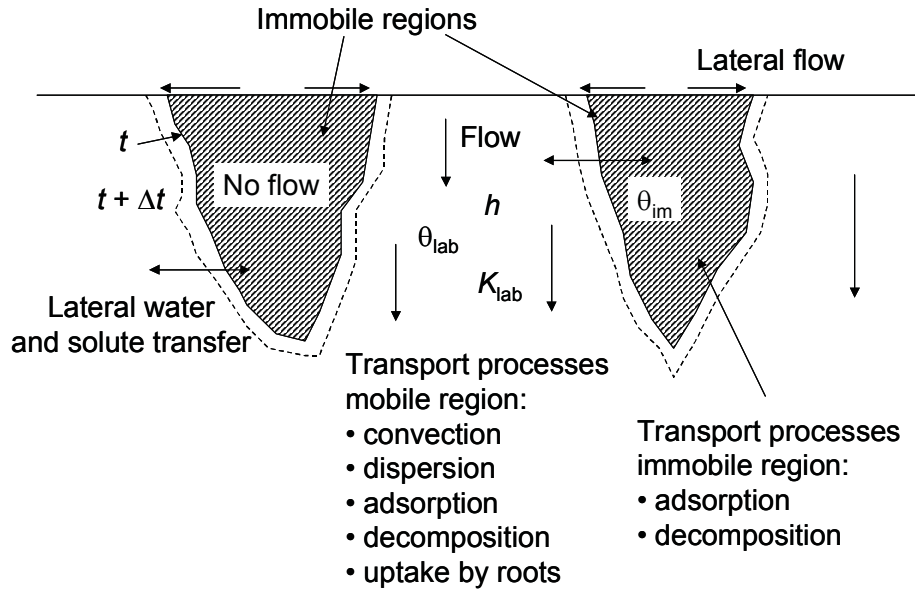


Figure 30 Schematization of mobile and immobile regions for flow and transport in water repellent soils

Richards' equation only applies to the mobile region. Therefore the effective retention function, which is used to solve Richards' equation, follows simply from:

$$\theta(h) = F_{\text{mob}}\theta_{\text{lab}}(h) \quad (6.7)$$

We may assume that the soil texture and the unsaturated hydraulic conductivity curves of the mobile and immobile regions are identical. In that case the soil water flux density q at a certain gradient $\partial H/\partial z$ will be reduced by the factor F_{mob} due to the reduction in flow domain. Thus, the effective field conductivity curve $K(h)$ which should be used in the solution of Richards' equation, is related to $K_{\text{lab}}(h)$ measured in the laboratory as:

$$K(h) = F_{\text{mob}}K_{\text{lab}}(h) \quad (6.8)$$

In this way the acceleration of soil water flow due to a smaller flow volume is taken into account. The time needed for some lateral soil water flow at depths where F_{mob} either increases or decreases with depth, is neglected. This convergent or divergent flow would require a more complicated three-dimensional analysis, as e.g. performed by De Rooij (1996).

Field studies (Ritsema and Dekker, 1994) show that the mobile fraction F_{mob} varies in time. In general, when the soil becomes wetter, F_{mob} increases. We might approximate this by a

linear relationship between $\log(-h)$ and F_{mob} . Notice that when the immobile regions contain water, variation of F_{mob} with h induces exchange of water between the mobile and immobile soil volumes (Figure 30). This exchange is included as an extra loss term G_w in the Richards' equation:

$$\frac{\partial \theta}{\partial t} = \frac{\partial \left[K \left(\frac{\partial h}{\partial z} + 1 \right) \right]}{\partial z} - S_a + \frac{\partial F_{\text{mob}}}{\partial t} \theta_{\text{im}} \quad (6.9)$$

where S_a the actual rootwater extraction rate (d^{-1}) and the last term in the right hand side of Eq. (6.9) accounts for the water amount transferred (d^{-1}) from the immobile to the mobile region.

<i>Specify for each soil layer:</i>			
<i>Variable Code</i>	<i>Description</i>		<i>Default</i>
	PF1	first $\log(-h)$ value (-)	0.0
F_{mob}	FM1	mobile fraction at first $\log(-h)$ value (-)	1.0
	PF1	second $\log(-h)$ value (-)	3.0
F_{mob}	FM2	mobile fraction at second $\log(-h)$ value (-)	1.0
θ_{im}	THETIM	volumetric water content in immobile soil volume	0.0

6.5 Macropore flow

6.5.1 Introduction

In structured soils (clay and peat soils), flow occurs preferential through large pores or macropores in the unsaturated soil matrix, a process known as 'bypass flow' or 'short-circuiting' (Hoogmoed and Bouma, 1980). Due to the very rapid flow through these macropores solutes can reach large depths almost immediately after the start of a shower, bypassing the capacity of the soil matrix for storage, adsorption and transformation of potential pollutants. This macroporosity can be caused by shrinking and cracking of soil, by plant roots, by soil fauna, or by tillage operations. Because macropores may have a large impact on water flow and solute transport through the vadose zone they should be included in generally applied agrohydrologic models like SWAP. Empirical models incorporating the bypass through macropores in a simplified way can be calibrated for specific soil samples or fields. However, because of their empirical character, the use of these models for predictive purposes is limited. Models that simulate the general physical processes are more reliable for use in scenario studies. Unfortunately, detailed simulation of the physical transport processes in cracked and macroporous soils is not feasible, as the chaotic and dynamic morphology of each location would require a huge amount of data. We may therefore search for some systematic behaviour on a larger scale, in the same way as Darcy's law incorporates complicated, unpredictable pore geometry at a scale where a continuum of water, solid material and air applies. In experimental fields with cracked clay, various locations show at the same soil depth a large variability of water contents and solute concentrations (Beven and Germann, 1982; Bronswijk et al., 1995). Instead of trying to describe water flow and solute transport at the various locations, the field average behaviour

might be more easy to catch in a model. In order to make the model suitable for process and scenario analysis, concepts should be used that are generally applicable, thus physically based. Furthermore, model calibration requires a limited number of parameters, and preferably parameters that can be measured directly in the field.

The importance of shrinkage cracks was already shown by Bronswijk, who implemented a concept for preferential flow through shrinkage cracks in the FLOCR model (Bronswijk, 1988). A modified version of this concept was implemented in SWAP by Van Dam (2000) and is included in this version of SWAP as option 1 for macropore flow: Simple macropore flow (Par. 6.5.2). Hendriks et al. (1999) showed the importance of permanent or static macropores (e.g. structural cracks, worm and root holes) beside the dynamic shrinkage cracks, with an extended version of the macropore concept of FLOCR. An adapted version of this more general concept for macropore flow is now implemented in this version of SWAP as option 2 for macropore flow: Advanced macropore flow (Par. 6.5.3). This option is yet in the testing phase and therefore still under construction.

6.5.2 Simple macropore flow

6.5.2.1 Introduction

In the simple macropore flow model shrinkage cracks are the sole macropores that are considered. The shrinkage characteristic is used to describe the swelling and shrinking of a clay soil, including its crack volume and crack depth. Water flow and solute transport are described with basic physics, employing ordinary numerical procedures. The model concept was developed to simulate the field average behaviour of a field with cracks, rather than the flow and transport at a single plot. Van Dam (2000) applied the model to an extensive field experiment, which was performed and described by Bronswijk et al. (1995).

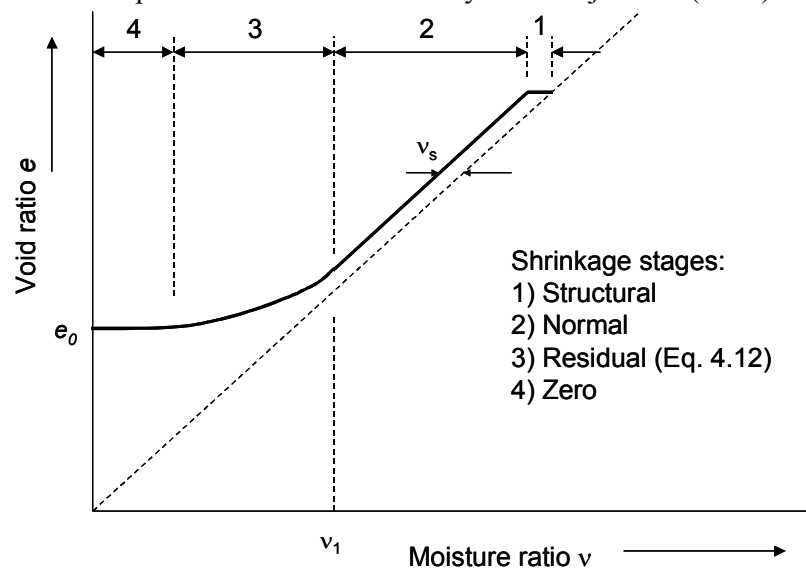


Figure 31 Void ratio e as function of moisture ratio v , showing four stages of a typical shrinkage characteristic (after Bronswijk, 1988)

6.5.2.2 Shrinkage characteristic

A shrinkage characteristic describes the relation between the amount of pores, as expressed by the void ratio, and the amount of water, as expressed by the moisture ratio (Bronswijk, 1988). The void ratio e ($\text{cm}^3 \text{cm}^{-3}$) is defined as:

$$e = \frac{V_p}{V_s} \quad (6.10)$$

and the moisture ratio v ($\text{cm}^3 \text{cm}^{-3}$) as:

$$v = \frac{V_w}{V_s} \quad (6.11)$$

where V_p is the total pore volume ($\text{cm}^3 \text{cm}^{-3}$) either filled with air or water, V_w the water volume ($\text{cm}^3 \text{cm}^{-3}$) and V_s the solid volume ($\text{cm}^3 \text{cm}^{-3}$). Figure 31 shows a typical shrinkage characteristic. Four stages can be distinguished (Stroosnijder, 1975; Bronswijk, 1988):

- 1) Structural shrinkage. When saturated soils dry, large water filled pores may be emptied. As a result, aggregates can get a somewhat denser packing. On the whole, the volume changes in this shrinkage phase are negligible, but water losses can be considerable.
- 2) Normal shrinkage. Volume decrease of clay aggregates is equal to moisture loss. The aggregates remain fully saturated.
- 3) Residual shrinkage. Upon drying the volume of the aggregates still decreases, but moisture loss is greater than volume decrease. Air enters the pores of the aggregates.
- 4) Zero shrinkage. The soil particles reached their densest configuration. Upon further moisture extraction, the volume of the aggregates remains constant. Moisture loss is equal to air volume increase of the aggregates. Rigid soils, like sands, only show this stage.

To facilitate input and data analysis in SWAP, an exponential relationship is employed for the residual shrinkage stage (Kim, 1992):

$$e = \alpha_{sh} e^{-\beta_{sh}v} + \gamma_{sh}v \quad (6.12)$$

with α_{sh} , β_{sh} , and γ_{sh} dimensionless, empirical parameters. The SWAP user needs to specify the void ratio e_0 at $v = 0$, the moisture ratio v_1 at the transition of residual to normal shrinkage, and the structural shrinkage, v_s (Figure 31). With these three input data, SWAP generates the parameters α_{sh} , β_{sh} , and γ_{sh} , and describes the $e(v)$ relationship.

Measured shrinkage characteristics of seven clay profiles in the Netherlands, as described by Bronswijk and Evers-Vermeer (1990), are listed in Appendix 5. Yule and Ritchie (1980a, 1980b) described shrinkage characteristics of eight Texas Vertisols, using small and large cores. Garnier et al. (1997) propose a simple evaporation experiment to determine simultaneously the moisture retention curve, hydraulic conductivity function and shrinkage characteristic.

The shrinkage characteristic enables us to calculate the crack volume and depth. Imagine a soil cube with sides z (cm) and volume $V = z^3$ (cm^3). In case of isotropic shrinkage of volume ΔV (cm^3) we may derive:

$$V = z^3, \quad V - \Delta V = (z - \Delta z)^3 \quad \text{and} \quad \Delta V = z^3 - (z - \Delta z)^3 \quad (6.13)$$

with Δz the change of each side length (cm). Therefore:

$$1 - \frac{\Delta V}{V} = \left(1 - \frac{\Delta z}{z}\right)^3 \quad (6.14)$$

In the case of one-dimensional subsidence without cracking, the following relation applies:

$$1 - \frac{\Delta V}{V} = \left(1 - \frac{\Delta z_{\text{ver}}}{z}\right)^1 \quad (6.15)$$

where Δz_{ver} is the vertical subsidence (cm). In a study on pedogenetically unripened soils, Rijniersce (1983) called the exponent in Eqs. (6.14) and (6.15) the geometry factor r_s . This results in a general relation between volume change ΔV and subsidence Δz_{ver} of a clay soil volume:

$$1 - \frac{\Delta V}{V} = \left(1 - \frac{\Delta z_{\text{ver}}}{z}\right)^{r_s} \quad (6.16)$$

In case of three-dimensional isotropic shrinkage, $r_s = 3$. When cracking dominates subsidence $r_s > 3$, when subsidence dominates cracking $1 < r_s < 3$. In case of subsidence only, $r_s = 1$.

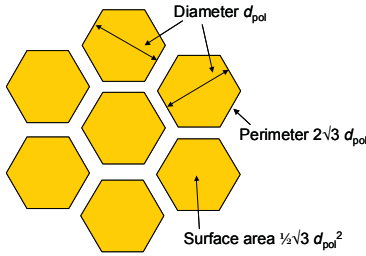


Figure 32 Geometry of soil matrix hexagons at a cracked clay soil

In order to calculate the lateral infiltration rate of water collected in cracks, we need to derive the vertical crack wall area. Consider a crack pattern of hexagons with diameter d_{pol} (cm) as depicted in Figure 32. We may derive that per unit depth the relative area of the vertical crack walls with respect to the horizontal surface area, $A_{\text{wall,rel}}$ ($\text{cm}^2 \text{ cm}^{-2}$), equals:

$$A_{\text{wall,rel}} = \frac{2\sqrt{3} d_{\text{pol}}}{\frac{1}{2}\sqrt{3} d_{\text{pol}}^2} = \frac{4}{d_{\text{pol}}} \quad (6.17)$$

6.5.2.3 Water flow concept

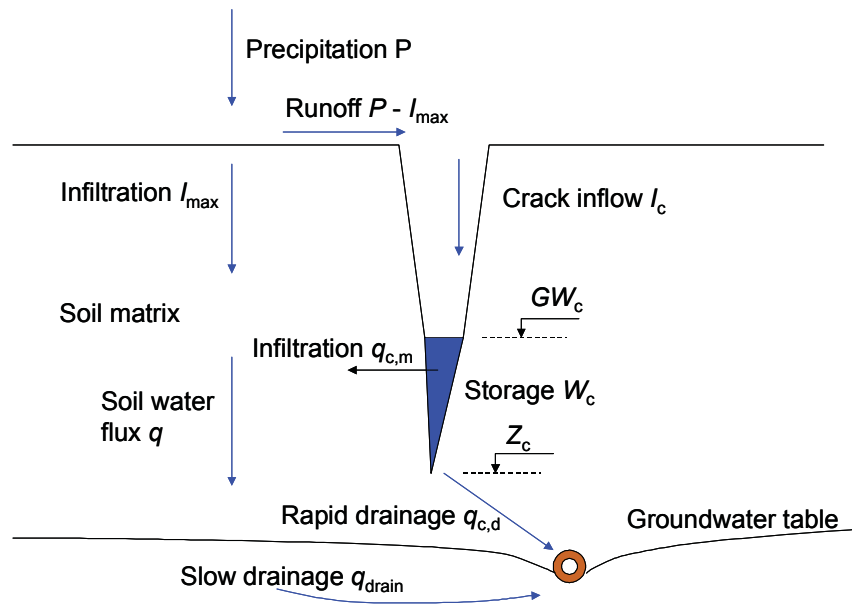


Figure 33 Concept of water flow in a cracked clay soil as applied in the simple macro pore concept. The variables are explained in the text.

The matrix and crack infiltration at a given rainfall intensity P can be calculated as (Bronswijk, 1988):

$$\begin{aligned}
 P < I_{\max} : \quad I_m &= A_m P \\
 &I_c = A_c P \\
 P > I_{\max} : \quad I_m &= A_m I_{\max} \\
 &I_c = A_m (P - I_{\max}) + A_c P
 \end{aligned}
 \tag{6.18}$$

with P the rainfall intensity (cm d^{-1}), I_{\max} the maximum infiltration rate of the soil matrix (cm d^{-1}), I_m the infiltration rate into the soil matrix (cm d^{-1}), I_c infiltration rate into the cracks (cm d^{-1}), and A_m and A_c relative areas of soil matrix and cracks, respectively ($\text{cm}^2 \text{cm}^{-2}$).

Figure 33 shows the concept of water flow in a cracked clay soil as implemented in SWAP. Precipitation in excess of the infiltration rate flows as runoff to the cracks, as described by Eq. (6.18). The time needed for ponding water to flow on the soil surface to the cracks is probably negligible. A small time delay can be created by defining a threshold ponding height, which should be reached before runoff to the cracks starts. The maximum infiltration rate I_{\max} is derived from an accurate solution of Richards' equation near the soil surface (see Par. 2.2). In order to do so, the nodal spacing near the soil surface should not exceed 1 cm, and the saturated hydraulic conductivity K_{sat} should be determined for the clay

matrix without cracks. Actual rainfall rates should be used, as daily rainfall rates underestimate seriously runoff amounts to the cracks.

Using the shrinkage characteristic and the actual water contents, the following steps are made to derive the amount of shrinkage ΔV , subsidence Δz_{ver} and relative, horizontal crack area A_c ($\text{cm}^2 \text{cm}^{-2}$) at a certain soil depth or node i :

- 1) Solid volume $V_s = 1.0 - \theta_{sat}$, where θ_{sat} is saturated water content ($\text{cm}^3 \text{cm}^{-3}$) of the considered soil layer;
- 2) Moisture ratio $\nu = \theta_i / V_s$, with the water content θ_i ($\text{cm}^3 \text{cm}^{-3}$) of node i , following from the solution of the Richards' equation at this time step;
- 3) Calculate void ratio e from the specified shrinkage characteristic $e(\nu)$;
- 4) Total pore volume $V_p = e V_s$;
- 5) Shrinkage soil volume with respect to maximum soil volume $\Delta V = \theta_{sat} - V_p$; vertical subsidence Δz_{ver} follows from Eq. (6.16);
- 6) Volume vertical crack $V_c = \Delta V - 1.0 \Delta z_{ver}$ ($\text{cm}^3 \text{cm}^{-3}$);
- 7) Relative horizontal crack area $A_c = 1.0 V_c / (1.0 - \Delta z_v)$ ($\text{cm}^2 \text{cm}^{-2}$).

In this procedure the water contents of the soil matrix are not adjusted for the shrinkage itself, which will change the vertical and horizontal co-ordinates. A study by Peerboom (1987) showed that the effects of these co-ordinate changes on simulated water contents and soil water movement inside the clay matrix are minor, while the numerical coding of this correction is substantial. Therefore this correction has been skipped, which results in the above listed straightforward procedure.

According to the described theoretical shrinkage characteristic (Figure 31), a crack volume would exist when $\theta_i < \theta_{sat}$. This would imply that as soon as the clay matrix is unsaturated ($h < 0$) cracks are formed. Field soils may deviate from this behaviour, showing crack bottoms higher and lower than the groundwater level. In the SWAP program we took this into account by calculating a crack volume if $\theta < \theta_{crit}$, where θ_{crit} is the critical water content for cracking derived from measurements. The concept of the shrinkage characteristic does not allow for the existence of cracks below the groundwater level ($\theta_{crit} \leq \theta_{sat}$), which is maintained in the SWAP program. In this way the level of the crack bottom Z_c is calculated as function of time.

Water collected in the cracks, will either infiltrate laterally to the soil matrix or flow rapidly to nearby drains and/or ditches, as depicted in Figure 33. The infiltration rate $q_{c,i}$ (cm d^{-1}) at node i can be derived straight from Darcy, if we assume a linear lateral pressure gradient in the soil matrix polygon and infiltration from each side:

$$q_{c,i} = -K(h_i) \frac{\partial H}{\partial x} = -6K(h_i) \frac{(h_i - h_{c,i})}{d_{pol}} \quad (6.19)$$

where K is the unsaturated hydraulic conductivity (cm d^{-1}), H the soil hydraulic head (cm), x the horizontal distance (cm), and h_i and $h_{c,i}$ are the nodal water pressure heads (cm) in the soil matrix and in the crack, respectively. The factor 6 accounts for water adsorption from all sides in the horizontal plane of the polygon. The water level in the cracks, GW_c (cm), can be calculated using the crack volume as function of depth as described earlier and the actual

crack water storage. The total lateral infiltration rate, $q_{c,m}$ (cm d⁻¹), is derived by the summation (Figure 33):

$$q_{c,m} = \sum_{z=Z_c}^{z=GW_c} q_{c,i} A_{\text{wall,rel}} \quad (6.20)$$

where Z_c is the crack depth (cm). The lateral infiltration rate is added as a source term $q_{c,i}/\Delta z_i$ to the Richards' equation for the water movement in the clay matrix:

$$\frac{\Delta \theta_i}{\Delta t} = \frac{\Delta}{\Delta z_i} \left[K(h_i) \left(\frac{\Delta h_i}{\Delta z_i} + 1 \right) \right] - S_a(h_i) + \frac{q_{c,i}}{\Delta z_i} \quad (6.21)$$

where S_a is the root water extraction rate (cm³ cm⁻³ d⁻¹). Field observations show that in cracked clay fields, water may flow directly from the cracks to drains or ditches, without entering the soil matrix. Hendriks et al. (1999) discussed an extensive concept for this so-called rapid drainage rate. In SWAP the rapid drainage rate, $q_{c,d}$ (cm d⁻¹), is calculated as function of the water collected in the cracks and with a linear rate coefficient f_{rapid} (d⁻¹):

$$q_{c,d} = f_{\text{rapid}} W_c \quad (6.22)$$

where W_c is the crack water storage (cm). Finally the change of water storage in the cracks, ΔW_c (cm), follows from the balance (Figure 33):

$$\Delta W_c = (I_c - q_{c,m} - q_{c,d}) \Delta t \quad (6.23)$$

Note that different from the earlier concept of Hoogmoed and Bouma (1980), water adsorption above the water level in the cracks is not included. Bouma and Dekker (1978) already concluded that the contact area between preferential flow and soil matrix forms only a small fraction of the total area available in the vertical ped surfaces. This complicates the calculation of horizontal adsorption. Booltink and Bouma (1993) applied the model with water adsorption to soil types ranging from loamy sand to clay and found that the lateral adsorption during bypass flow was always less than 1 percent. Therefore lateral adsorption was not included in this simple macropore model.

<i>Model input</i>			
<i>Variable</i>	<i>Code</i>	<i>Description</i>	<i>Default</i>
e_0	SHRINA	void ratio at zero water content (cm ³ cm ⁻³)	
v_1	MOISR1	moisture ratio at transition residual to normal shrinkage (cm ³ cm ⁻³)	
v_s	MOISRD	amount of structural shrinkage (cm ³ cm ⁻³)	
	ZNCRACK	depth at which crack area of soil surface is calculated (cm)	-5.0
r_s	GEOMF	geometry factor (-)	3.0
d_{pol}	DIAMPOL	diameter of soil matrix polygon (cm)	
f_{rapid}	RAPCOEF	rate coefficient of bypass flow from cracks to surface water (d ⁻¹)	
<i>Specify for each soil layer:</i>			
	THETCR	critical water content below which cracks are formed (cm ³ cm ⁻³)	

6.5.3 Advanced macropore flow

6.5.3.1 Introduction

It is known from the literature that other forms of macropores besides shrinkage cracks, such as structural cracks and worm and root holes, are of major importance for preferential flow in structured soils (see Hendriks et al., 1999). Therefore, the advanced macropore flow concept in SWAP contains these permanent macropores as well as temporary shrinkage cracks. This approach was taken from an adapted version of the FLOCR model (Hendriks et al., 1999) and is now implemented in SWAP. This option is yet in the testing phase and therefore still under construction. This applies as well to the description of this concept.

In many models, vertical water transport through macropores is calculated with Poiseuille's law and lateral infiltration into the unsaturated matrix of water trapped in non-continuous macropores at different depths (internal catchment) is accounted for by a tortuosity factor (e.g. Beven and Germann, 1981, Jarvis, 1989). In the SWAP model, a different approach is implemented, that is based on the geometry of the macropore structure. In this approach water flowing into the macropores is instantaneously added to the water storage at the bottom of the macropores. Lateral infiltration into crack walls of water running rapidly downwards along cracks is neglected, since according to Hoogmoed and Bouma (1980) and Booltink (1993) this infiltration is small. However, some of the macropore inflow will be trapped in non-continuous macropores and is therefore forced to infiltrate into the unsaturated matrix at different depths. Bouma and Dekker (1978), Van Stiphout et al. (1987) and Bouma (1990) call this process 'internal catchment'. In SWAP this process is explicitly implemented on the basis of the description of the macropore geometry.

6.5.3.2 Macropore geometry

In order to describe the geometry of the macropore structure the macropore volume is partitioned according to two properties:

I. Continuity:

- 1) main bypass flow domain: a network of continuous macropores (structural and shrinkage cracks);
- 2) internal catchment domain: discontinuous macropores ending at different depths;

II. Persistency:

- 1) static macropore volume: macropores that are permanent present;
- 2) dynamic macropore volume: shrinkage cracks.

Two classes of macropore are distinguished with respect to pore continuity. The first domain represents the main system of continuous and interconnected structural and shrinkage cracks that penetrate relatively deeply into the soil profile (i.e. the main bypass domain). The second domain represents macropores ending at different depths in the profile, resulting in 'internal catchment' (i.e. the internal catchment domain). Figure 34 shows a conceptual visualisation of these two classes of macropores. As shown in this figure, the volume of macropores in the main bypass domain consists of a network of interconnected macropores (e.g. structural and shrinkage cracks). It is constant with depth up to the depth where the internal catchment domain stops; thereafter the volume of pores in the main bypass domain decreases linearly with depth. The volume of the internal catchment consists of macropores that are not interconnected and that end at different

depths. The decline of the number of internal catchment macropores is described by a power law function (Figure 35). The internal catchment domain can be divided in a number of subdomains (horizontal discretisation). For each (sub)domain, the macropores in the various compartments are vertically interconnected.

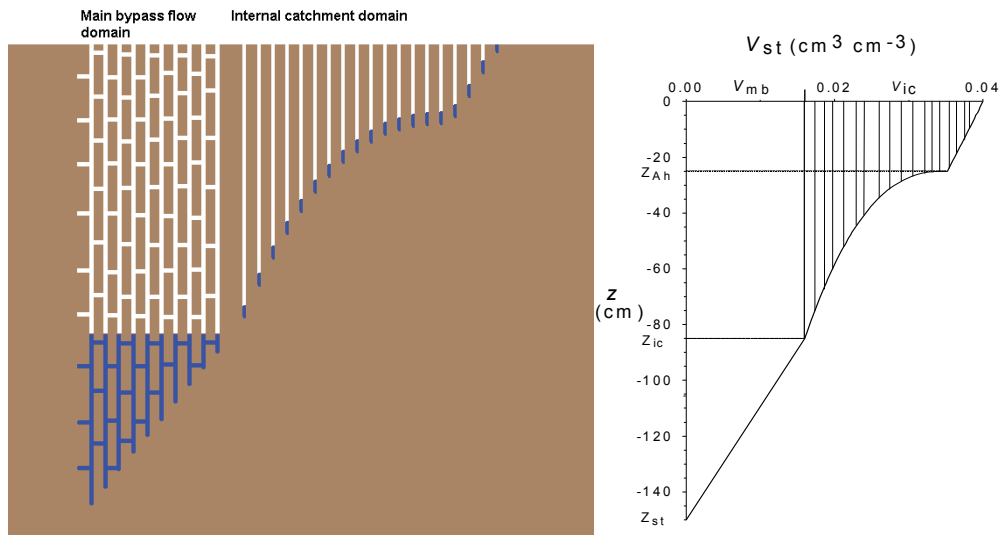


Figure 34 Schematic representation of the 2 domains: 1) main bypass flow domain (left part): transporting water and solutes deeper into profile and rapid drainage, 2) internal catchment (right part) domain: infiltration of trapped water into unsaturated matrix at different depths. The figure on the left gives a graphical representation of the two domains.

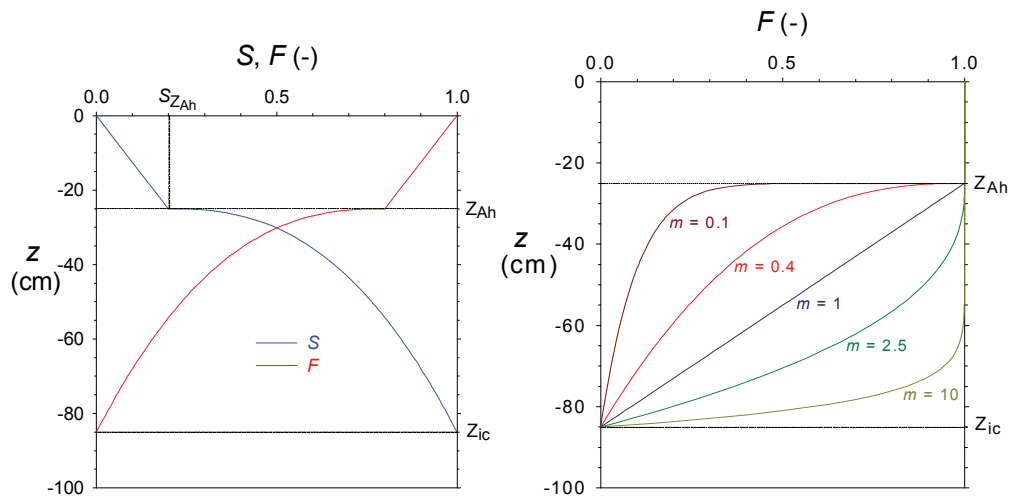


Figure 35 The decline of the number of internal catchment macropores is described by a power law function with power m . $m = 1$ represents a linear decline, while $m < 1$ represents a shallow system and $m > 1$ a deep system. ' $S_{Z_{Ah}}$ ' in the figure is similar to ' $R_{Z_{Ah}}$ ' in the list of Model input in 6.4.3.4.

Two types of macropore are included in the model to describe the dynamics of the macropore volume resulting from swelling and shrinking: a permanent static macropore volume independent of the soil moisture status and dynamic shrinkage cracks whose volume depends on the shrinkage characteristic and the current soil moisture content.

SWAP simulates the swelling and shrinking dynamics via a simplified procedure: the soil level remains fixed and swelling and shrinking influences only the pore volumes. For clay Eq. (6.12) is used to describe the shrinkage characteristic, and consequently the same input parameters are required as described in Par. 6.5.3.4. The shrinkage characteristic of peat differs strongly from the characteristic of clay. An analytical function for describing the peat characteristic is being developed. Figure 36 visualises the static and the dynamic macropore volumes. For each model compartment, a fraction of the volume per unit of horizontal area is considered to represent static macropores. In compartments with shrinkage cracks, the volume of the permanent macropores is added to the volume of the shrinkage cracks, resulting in a total macropore volume.

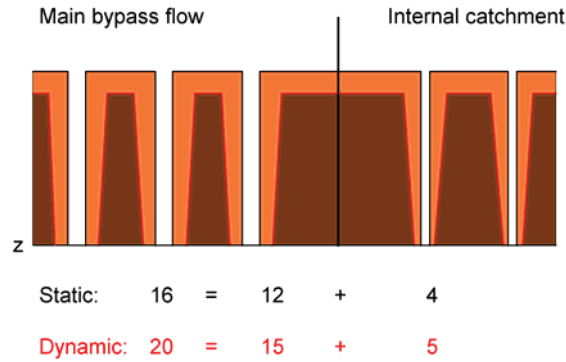


Figure 36 Partition between static and dynamic macropore volume: white area represents static and grey area dynamic macropor volume. Dark colour is the soil matrix.

6.5.3.3 Water flow

Figure 37 illustrates the different water flows into and from macropores in the SWAP advanced macropore concept. The amount of water routed into the macropores (I_{mp1} and I_{mp2}) at a given rainfall intensity P is calculated as described by Bronswijk (1988):

$$\begin{aligned}
 P \leq I_{\max} : \quad & I_m = A_m P \\
 & I_{mp1} = 0 \\
 & I_{mp2} = A_{mp} P \\
 P > I_{\max} : \quad & I_m = A_m I_{\max} \\
 & I_{mp1} = A_m (P - I_{\max}) \\
 & I_{mp2} = A_{mp} P \\
 I_{mp} &= I_{mp1} + I_{mp2}
 \end{aligned} \tag{6.24}$$

with P the rainfall intensity (cm d^{-1}), I_{\max} the maximum infiltration rate of the soil matrix (cm d^{-1}), I_m the infiltration rate into the soil matrix (cm d^{-1}), I_{mp} total infiltration rate into the macropores (cm d^{-1}), and A_m and A_{mp} relative areas of soil matrix and macropores, respectively ($\text{cm}^2 \text{cm}^{-2}$).

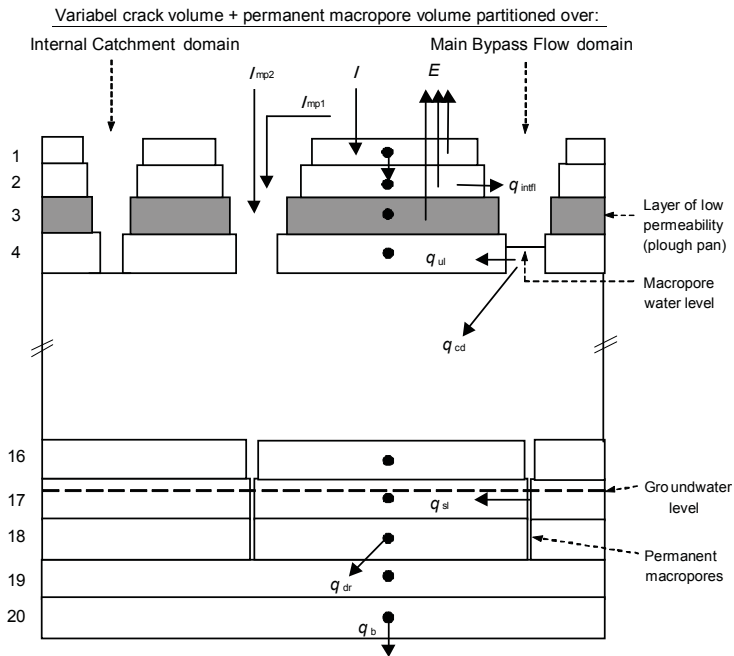


Figure 37 Schematic representation of the soil profile with the soil matrix, divided in 20 model compartments, and macropores and the various water fluxes ($m d^{-1}$) within the soil profile: I is infiltration rate into the soil matrix, I_{mp1} is part of total crack infiltration caused by rainfall intensity exceeding the maximum infiltration rate of the soil matrix, I_{mp2} is part of total crack infiltration caused by rain falling directly into the cracks, E is actual evapotranspiration, q_i is Darcy flux between two nodal points, q_b is bottom boundary flux, q_{inft} is interflow over layer of low permeability into macropores, q_{cd} is drainage flux via cracks, q_{ul} is lateral infiltration out of macropores into unsaturated matrix, q_{sl} is lateral infiltration out of macropores into saturated matrix.

The distribution of the total inflow into the macropores at the soil surface over the different domains is determined by the ratio of the volume fractions of the domains in the first compartment. Water flowing into the macropore domains accumulates at the bottom of the macropores. Some of the stored water can infiltrate laterally into the soil matrix that is in contact with this water, and, only in the case of the first domain, some of it can drain rapidly to the drainage systems. Water that has not infiltrated or drained within one time step is saved as storage for the next time step. A separate water balance is calculated for each (sub)domain. From saturated model compartments, water can exfiltrate into the macropores if the water potential in the macropores is lower than that in the soil matrix. This can happen in the case of a rising groundwater table in the matrix, but also when top compartments overlying a soil layer of relatively low permeability (e.g. a plough pan) become saturated and interflow occurs from these compartments into the macropores.

Unsaturated lateral infiltration

The calculation of the lateral infiltration through the macropore wall into the unsaturated soil compartments is based on the sorptivity (Philip, 1957):

$$I_{ul,i}(t) = \frac{4 S_i(\theta_{0,i}) \sqrt{t - t_{0,i}}}{d_{a,i}} D_i \quad (6.25)$$

where i is the compartment number; $I_{ul,i}$ is the unsaturated lateral infiltration (m), cumulative from time $t = t_{0,i}$ to $t = t$ (d); $S_i(\theta_{0,i})$ is Philip's sorptivity ($\text{cm d}^{-0.5}$) as a function of $\theta_{0,i}$, the initial volumic water content ($\text{cm}^3 \text{cm}^{-3}$) at $t = t_{0,i}$ the time of first contact of macropore water with the matrix; $d_{a,i}$ is the diameter of the aggregates (cm) and D_i is the thickness of the compartment (cm).

Sorptivity as a function of the initial volumic water content $\theta_{0,i}$ is derived from an empirical relation developed by Greco et al. (1996):

$$S_i(\theta_{0,i}) = S_{d,i} \left(1 - \frac{\theta_{0,i}}{\theta_{s,i}} \right)^{\alpha_i} \quad (6.26)$$

where $S_{d,i}$ is the sorptivity when $\theta_{0,i} = 0$; $\theta_{s,i}$ is the volumic water content at saturation; α_i is a fitting parameter (-).

The infiltration rate during the time step Δt is linearised to obtain an average, constant rate $q_{ul,i}(t)$ (cm.d^{-1}):

$$q_{ul,i}(t) = - \frac{I_{ul,i}(t + \Delta t) - I_{ul,i}(t)}{\Delta t} \quad (6.27)$$

The advantage of this approach is that measured values can be used for the sorptivity in relation to the initial moisture content. These measured sorptivities reflect the influence of water-repellent coatings on the surface of the clay aggregates which often hamper infiltration into these aggregates (Thoma et al., 1992; Dekker and Ritsema, 1996). If measured sorptivities are not available, the sorptivity in relation to the moisture content can be derived from the soil hydraulic functions (Parlange, 1975).

Saturated lateral infiltration

From the permanent macropores below the groundwater table, water can infiltrate laterally into the saturated matrix. The infiltration rate can be described by Darcy's law:

$$q_{sl,i} = - \frac{\delta k_{s,i} D_i h_{mg}}{d_{ap,i}^2} \quad (6.28)$$

where $q_{sl,i}$ is the saturated lateral infiltration flux (cm d^{-1}); $k_{s,i}$ is the saturated hydraulic conductivity (cm d^{-1}); D_i is the thickness of the compartment (cm); h_{mg} is the difference in potential (cm) between the water in the macropores and the groundwater; $d_{ap,i}$ is the effective diameter (cm) of aggregates in the zone with permanent macropores.

If the matrix water potential is higher than the macropore water potential, h_{mg} is negative and exfiltration from the matrix into the macropores occurs.

Rapid drainage

Rapid drainage via a network of cracks is calculated according to the drainage theory with one calibration parameter: the reference drainage resistance γ_{ref} (d^{-1}) for rapid drainage at field capacity (pF = 2). The rapid drainage flux q_{cd} (cm d^{-1}) is calculated from the crack water level h_{cd} (cm) above drain level and the actual drainage resistance γ_{act} (d^{-1}) at actual moisture content:

$$q_{cd} = \frac{h_{cd}}{\gamma_{\text{act}}} \quad (6.29)$$

The actual drainage resistance is calculated from the reference drainage resistance according to the ratio between actual and reference (at $pF = 2$) transmissivity kD ($\text{cm}^2 \text{d}^{-1}$):

$$\gamma_{\text{act}} = \frac{kD_{\text{ref}}}{kD_{\text{act}}} \gamma_{\text{ref}}, \text{ with} \quad (6.30)$$

$$kD_{\text{ref}} = \sum_{i=1}^{nd} k_{\text{ref},i} D_i \quad \text{and} \quad kD_{\text{act}} = \sum_{i=nt}^{nb} k_{\text{act},i} D_i$$

nd and nb are the numbers of respectively the compartment with the drainage level and the bottom compartment with water in macropores. The horizontal saturated hydraulic conductivity of the cracks k_i (cm d^{-1}) is a function of the dynamic crack width and as such is based on a slit model presented by Bouma and Anderson (1973) with r (-) is a reaction coefficient that determines the reaction of k to changes of the crack width w_i (with C is a system depending constant):

$$k_{\text{ref},i} = C \frac{(w_{\text{ref},i})^r}{d_i} \quad \text{and} \quad k_{\text{act},i} = C \frac{(w_{\text{act},i})^r}{d_i} \quad (6.31)$$

The crack width $w_{c,i}$ (cm) can be calculated from the relative volume of cracks $V_{c,i}$ ($\text{cm}^3 \text{cm}^{-2}$):

$$w_{c,i} = d_a \left(1 - \sqrt{1 - \frac{V_{c,i}}{D_i}} \right) \quad (6.32)$$

The diameter d_i of the soil polynomes (cm) per compartment i is calculated from the maximum d_{max} and minimum diameter d_{min} , and the number of domains $N_{d,i}$ in compartment i and the maximum number of domains $N_{d,\text{max}} = 1 + N_{\text{sd}}$ (number of subdomains in internal catchment domain):

$$d_i = d_{\text{min}} + \frac{N_{d,\text{max}} - N_{d,i}}{N_{d,\text{max}} - 1} \cdot (d_{\text{max}} - d_{\text{min}}) \quad (6.33)$$

All flows out of the macropores occur simultaneously. The distribution of drainage and the two forms of lateral infiltration depends on the rates of these processes.

6.5.3.4 Parameterisation of model input

<i>Model input</i>			
<i>Variable</i>	<i>Code</i>	<i>Description</i>	<i>Default</i>
Z_{Ah}	Z_Ah	depth bottom A-horizon (cm)	
Z_{Ic}	Z_Ic	depth bottom Internal Catchment (IC) domain (cm)	
Z_{St}	Z_St	depth bottom static macropores (cm)	
$V_{St,0}$	VIMpStSs	volume of static macropores at soil surface ($\text{cm}^3 \text{cm}^{-3}$)	
$P_{Ic,0}$	PpIcSs	proportion of IC domain at soil surface (-)	
N_{sd}	NumSbDm	number of subdomains in IC domain (-)	
m	PowM	power M for frequency distribut. curve IC domain (-)	1.0
R_{ZAh}	RZAh	fraction macropores ended at bottom A-horizon (-) Optional	0.0
S	Spoint	symmetry point for freq. distr. curve (-) Optional	1.0
-	SwPowM	switch for double convex/concave freq. distr. curve (-) Optional	0
d_{min}	DiPoMi	minimal diameter soil polygons (shallow) (-)	
d_{max}	DiPoMa	maximal diameter soil polygons (deep) (-)	
-	ZnCrAr	depth at which crack area of soil surface is calculated (cm)	-5.0
-	CofAniMp	coefficient of anisotropy for Ksat	1.0
-	SwDrRap	switch for kind of drainage function TEMPORARY: TEST (-)	
γ_{ref}	RapDraResRef	reference rapid drainage resistance (d^{-1})	
r	RapDraReaCof	reaction coefficient for rapid drainage (-)	
<i>Specify for each soil layer:</i>			
-	SwSoilShr	switch for kind of soil for determining shrinkage curve (-): 0 = rigid soil, 1 = clay, 2 peat	
-	SWSshrInp	switch for determining shrinkage curve (-): 1 = parameters for curve; 2 = typical points of curve	
-	ThetCrMP	critical water content below which cracks are formed ($\text{cm}^3 \text{cm}^{-3}$)	
r_s	GeomFac	geometry factor (-)	3.0
-	ShrParA - ShrParE	5 possible parameters for describing shrinkage characteristics	
-	SWSorp	switch for kind of sorptivity function (-) 0 = Parlange, 1 = sorptivity curve	
-	SorpFacParl	factor for modifying Parlange function (-)	1.0
$S_{d,i}$	SorpMax	maximal sorptivity at theta residual ($\text{cm d}^{0.5}$)	
α_i	SorpAlfa	fitting parameter for empirical sorptivity curve (-)	

6.5.3.5 Output for solute transport models

Output of this module can be used as hydrological input in other models. For this purpose all in- and outgoing flows from matrix compartments, macropore domains and drains are accumulated over each output interval. In order to limit the total output, the water balance terms of the internal catchment macropore domains are lumped together in one domain (Appendix 16). The purpose of distinguishing different domains to describe internal catchment is to allow simulation of lateral infiltration and macropore water storage at increasing depths. Water flowing into the different domains basically has the same solute concentration, which will only change during storage. It is assumed that the storage time in

the shallow internal catchment domains is relatively small. For the purpose of calculating solute transport, therefore these domains can be treated as one integrated domain without introducing large errors. Since the storage time in the deep first domain, which often penetrates into the groundwater, is much larger, it remains necessary for solute transport simulation to distinguish this domain from the integrated internal catchment domain.